Eur J Nucl Med Mol Imaging (2008) 35:821–837
DOI 10.1007/s00259-007-0631-y

REVIEW ARTICLE

Current concepts on imaging in radiotherapy

Michela Lecchi · Piero Fossati · Federica Elisei · Roberto Orecchia · Giovanni Lucignani

Received: 28 May 2007 / Accepted: 2 October 2007 / Published online: 31 October 2007

Abstract New high-precision radiotherapy (RT) techniques, such as intensity-modulated radiation therapy (IMRT) or hadrontherapy, allow better dose distribution within the target and spare a larger portion of normal tissue than conventional RT. These techniques require accurate tumour volume delineation and intrinsic characterization, as well as verification of target localisation and monitoring of organ motion and response assessment during treatment. These tasks are strongly dependent on imaging technologies. Among these, computed tomography (CT), magnetic resonance imaging (MRI), ultrasonography (US) and positron emission tomography (PET) have been applied in high-precision RT. For tumour volume delineation and characterization, PET has brought an additional dimension to the management of cancer patients by allowing the incorporation of crucial functional and molecular images in RT treatment planning, i.e. direct evaluation of tumour metabolism, cell proliferation, apoptosis, hypoxia and angiogenesis. The combination of PET and CT in a single imaging system (PET/CT) to obtain a fused anatomical and functional dataset is now emerging as a promising tool in radiotherapy departments for delineation of tumour volumes and optimization of treatment plans. Another exciting new area is image-guided radiotherapy (IGRT), which focuses on the potential benefit of advanced imaging and image registration to improve precision, daily target localization and monitoring during treatment, thus reducing morbidity and potentially allowing the safe delivery of higher doses. The variety of IGRT systems is rapidly expanding, including cone beam CT and US. This article examines the increasing role of imaging techniques in the entire process of high-precision radiotherapy.

Keywords PET/CT · MRI · Image registration · Radiation treatment planning · Precision radiotherapy

M. Lecchi · P. Fossati · F. Elisei · R. Orecchia · G. Lucignani (✉)
Institute of Radiological Sciences, University of Milan,
Via Di Rudinì, 8 20142 Milan, Italy
e-mail: giovanni.lucignani@unimi.it

M. Lecchi · F. Elisei · G. Lucignani
Unit of Nuclear Medicine, San Paolo Hospital,
Milan, Italy

P. Fossati · R. Orecchia
CNAO Foundation,
Milan, Italy

R. Orecchia
Department of Radiation Oncology,
European Institute of Oncology,
Milan, Italy

Introduction

Radiotherapy (RT) continues to play a key role in the management of cancer patients. A marked technological improvement in RT has attracted interest from related fields and encouraged experimental and theoretical studies which, in turn, have led to a better management of treatment modalities.

Radiation deposits energy into the patient's body. When cells absorb too much energy, they can be damaged and lose their reproductive capability. RT directed against cancer cells also affects normal cells along the radiation path. So a key issue in RT treatment is how to deliver the prescribed radiation dose to cancer cells, while keeping the dose to normal cells as low as possible.

Over the past decade, sophisticated dose delivery techniques, like intensity-modulated radiation therapy (IMRT) [1], stereotactic RT and hadrontherapy (particle beams) [2], along with more accurate dose calculation algorithms, have allowed precisely sculpting of the radiation dose to volumes of almost any shape.

A typical process of these high-precision RT techniques consists of five major phases: (1) simulation, (2) treatment planning, (3) set-up verification, (4) beam delivery and (5) response assessment.

In the simulation procedure, the patient is positioned (using optical lasers) and immobilized just as he/she will be during treatment delivery. The patient's structural information is obtained using computed tomography (CT). The CT images, containing three-dimensional (3D) information of patient anatomy, are then transferred to an RT planning (RTP) system for the treatment planning step in which tumour extension and organ at risks (OARs) are identified and the target volume to be treated is defined.

During this phase, the treatment parameters are determined according to the volumes defined on images and dose prescription. Once a plan that meets the criteria is calculated, the parameters of the plan are automatically transferred to the treatment machine.

In the third phase, the patient is positioned on the treatment table for each treatment session in the same way as was done during the simulation. This presumes that any components affecting the reproducibility of patient positioning during the course of treatment are known and corrected as needed.

In the fourth phase, the beam delivery stage, the machine is operated according to the plan parameters. In selected cases, such as lung and liver lesions, this step can take advantage of real-time assessment of tumour position.

Finally, the fifth phase regards the assessment of tumour response after RT, important in determining treatment success and in guiding future patient therapy.

Nowadays, the success of the first three steps of the high-precision RT process requires the use of imaging to provide both anatomical and functional information [3], and even the last phases can rely on imaging for organ motion control (gating and tracking), for real-time in vivo dosimetry and tumour response assessment. More and more often, CT is registered with other imaging modalities, such as magnetic resonance (MR) and positron emission tomography (PET) (Fig. 1).

The need of an accurate set-up verification has required the development of image-guided radiotherapy (IGRT), a process that extends beyond the simple management of inter- and intra-fraction motion as it involves most other steps in the RT process, including patient immobilization, simulation, treatment planning, plan evaluation, patient setup verification and correction, dose delivery and quality assurance [4, 5].

Phase 1: simulation

In this first phase there is the need to acquire information on the patient anatomy. The older approach relied on the two-dimensional (2D) conventional simulator. This is a device with an X-ray tube capable of the same mechanical movements of the treatment unit; this device is able to simulate the treatment employing a diagnostic low dose beam, hence the name "simulation".

The use of a 2D simulator alone cannot provide 3D information or direct visualization of soft tissue volumes and is therefore becoming increasingly obsolete. In modern RT, 3D imaging devices are employed. CT is the most widely used 3D imaging modality owing to its acceptable costs, wide availability and ability to provide tissue density information needed for dose calculation. The main requirements (Table 1) of a CT scanner in RT treatment planning are a flat couch and a wide aperture (at least 70 cm).

A CT scanner can be combined with a conventional simulator (physical simulation) or used alone for so called virtual simulation (VS), a term coined by Sherouse et al. about 20 years ago [6]. CT simulation and the development of the concept of VS have rendered faster and more precise this procedure than physical simulation [7, 8]. In addition,

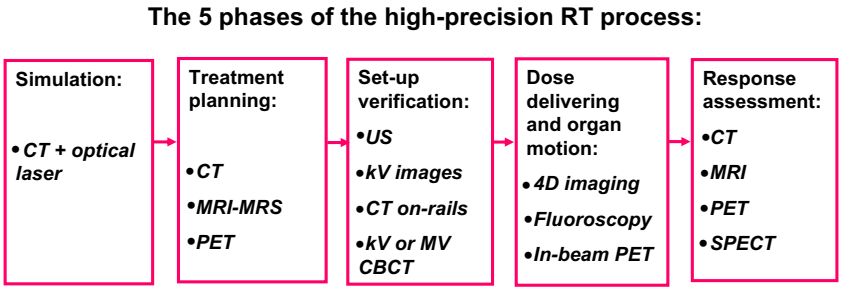

Fig. 1 Schematic view of the imaging modalities used or now investigated in the high-precision RT process (*CT* computed tomography, *MRI* magnetic resonance imaging, *MRS* magnetic resonance spectroscopy, *US* ultrasonography, *kV* kilovoltage, *MV* megavoltage, *CBCT* cone beam CT)

Table 1 Main features of a CT simulator for RT treatment planning

Feature	Specification
Aperture	Al least 70 cm
X-ray tube	80-130 kV; 250 to 500 kV
Minimum slice width	1 mm
Patient support	Table top identical to that used on treatment machine
Acquisition time	1–2 slice/rev s^{-1} (multi-slice 4 or 8 slice/rev s^{-1})
Laser accuracy	±1 mm
Accuracy of slice location	<1 mm

the use of CT scan images (in some case combined with other imaging studies, such as MRI or PET scan) represent the current standard for performing the steps involved in 3D conformal RT.

It is worth mentioning that the patient's physical examination by radiation therapists should be a part of the simulation procedure. Findings from physical examination can be integrated in CT images by the use of radio-opaque markers placed non-invasively on the patient's body surface at sites of a palpable mass, scars or other structures. Markers can also be used to show internal body cavities or orifices.

Phase 2: RT treatment planning

RTP consists of several steps: first of all, delineation of target volumes and organs at risk is obtained as defined by ICRU reports 50 and 62; then, dose constraints must be defined and lastly, a plan that meets the criteria must be calculated.

Simulation and treatment planning are two well-separated phases of RT, but are closely interrelated. Images acquired during the simulation or before the RTP should be used during planning and therefore the necessities of the planning phase determine the selection of the used imaging modalities. Table 2 shows the advantages and drawbacks of CT, MRI and PET imaging techniques in RTP.

The role of MR in target characterization

CT images are helpful for distinguishing between structures that have substantially different X-ray attenuation properties (air, tissue and bone), but it is difficult to discriminate soft tissue structures with similar attenuation unless there is a fat, air or bone interface between them. This limitation has led to significant inter- and intra-observer variations in tumours of the head and neck, lung, oesophageal, prostate, breast, cervical and brain [9–14]. Thus, in the clinical practice of radiotherapy, MRI is often routinely added to CT-based planning to improve target volume definition.

MRI provides excellent characterization of soft tissues and multi-planar capability [15]. The drawbacks of MRI are the lack of attenuation information and potential image distortion, although the possibility to estimate the electron density information from RM images was investigated recently with good results [16].

Efficient MR distortion assessment and CT co-registration programs can overcome these limitations and permit the use of MRI in RTP.

MRI has been used extensively for treating tumours of the central nervous system, where studies have reported quantitative improvements of up to 80% in target volume definition [17]. Because head and neck anatomy is highly complex, the extent of the infiltrating tumour may be difficult to define [18]. Treatment of tumour region such as the nasopharynx has been optimized with the integrated use of MRI [19]. In the pelvis, MRI has provided improved target delineation for urological [20] and gynaecological [21] cancers. In prostate cancer, comparative MRI-CT planning studies using MRI-defined prostate volumes as a gold standard have reported that CT-defined prostate volumes tend to overestimate the planning volume by 27–43% due to soft tissue uncertainty in CT delineation [22].

Unfortunately, although standard MRI scans are able to provide extremely detailed anatomic images, their findings do not always correlate with tumour biology. Thus, they do not always provide sufficient contrast to identify tumour extent or to identify regions of high cellular activity that might be targeted with boost doses.

MR provides numerous techniques for image-based surrogates of different function aspects: angiogenesis-perfusion MRI; metabolism-MR spectroscopy (MRS) and tissue at risk and tumour cellularity-diffusion weighted imaging [23].

Today, MRS is an emerging modality to identify the extent and position of tumours, aiding delineation of target volumes. MRS employs nuclear magnetic resonance techniques to investigate the metabolism of chemicals in the living body allowing the measurement of biochemical changes within the target volume, the detection of metabolic markers of different tumour phenotypes, and characterize tumour microenvironments in terms of blood volume and vessel permeability. Moreover, since the biochemistry of tumours is different from that of normal tissue, MRS has the potential to aid identification of tumours when there is insufficient contrast in the morphological images.

MRS is based on the fact that different chemicals containing the same nucleus exhibit characteristic chemical shifts in resonance frequency, allowing the chemical form of the element to be identified. The magnetic nuclei used to measure the MRS signals from the different metabolites are mainly ^{31}P or ^{1}H. ^{31}P-MRS searches information on metabolites involved in pathways up-regulated in cancer

Table 2 Advantages and disadvantages of CT, MRI and PET for radiotherapy planning

	CT	MRI	PET
Patient			
Advantages	Very fast scan with the potential to reduce motion artefacts	Not or minimally invasive procedure No radiation associated with imaging Potential both anatomical and biochemical information from MR spettroscopy	Both anatomical and functional information in a single study using PET/CT scanners
Drawbacks	Radiation associated with imaging (although RT patients entail much higher radiation exposure)	Claustrophobia due to the smaller patient bore Contraindicated in patients with loose metal foreign bodies within the body	Long acquisition scan Administration by intravenously injection of radiopharmaceutical compounds
Imaging			
Advantages	Very accurately spatial information	Superior soft tissue imaging with excellent spatial resolution	Providing functional and biological information
	Electron density information for dosimetry	True multiplanar capability to image in any oblique plane	May have diagnostic value detecting metastatic lesions that would have been missed on conventional imaging
	Cortical bone information to create digitally reconstructed radiographs (DDR)	Providing functional information (MR spectroscopy)	Asses locoreginal lymph node spread more precisely than CT
Drawbacks	Sub-optimal soft tissue imaging	MR image distortion	Limited spatial resolution and lesion detectability
	Lack of functional and biological information	Lack of electron density information for dosimetry	Important interobserver variability
		Lack of cortical bone information to create DDR	Variable effect of thresholds or other criteria used to define tumour margins
		Immobilization devices used in RT may not always be MR compatible	
Machine			
Advantages	High bore (85 cm) Flat table top	Open MR systems for easier patient access, tolerance and positioning for RT	Relative high bore (70 cm) Flat table top
Drawbacks	Shielding to avoid radiation exposure	Smaller bore than CT (50 cm) Curved table top	Shielding to avoid radiation exposure

and therefore ^{31}P MRS could play an important role in target identification, but the ^{31}P sensitivity is only 6% compared to ^{1}H at a fixed field strength. ^{1}H is the most sensitive magnetic nucleus because hydrogen is present in nearly all biologically relevant compounds. ^{1}H MRS metabolites include choline, citrate, lactate and creatine. However, efficient water and fat-suppression techniques are needed to suppress the large signal from tissue water and lipids.

The sensitivity and specificity of MRS techniques for cancer studies increased significantly in the last few years, causing new interest for their potential role as a tool for the definition of target sub-volumes at higher risk of failure after radical radiotherapy.

A number of groups investigated the sensitivity and specificity of MRS for locating prostate adenocarcinoma: MRS sensitivity was found to be within the range 38.5 to 77%, and specificity was found to be between 38.5 and 78%. Combined MRI/MRS had increased sensitivity up to 100% [24].

The use of MRS in radiotherapy is currently under evaluation mainly in brain (where MRS has been shown to differentiate between many tumour types and grades) and in prostate (where cancer may be distinguished from normal tissue and benign prostatic hypertrophy) [25].

In the last case, MRS has been used in combination with MRI to define regions for dose escalation within the

prostate permitting a dose >90 Gy to the tumour area respect to the whole prostate treated with a homogenous dose of about 70 Gy [26].

However, MRS use in RTP is in its infancy and the biological and technical pitfalls of MRS need to be underlined before its introduction into routine clinical practice. For example, an important disadvantage of ^{1}H MRS is that the signals from metabolites are relatively small, so the in-vivo resolution is poor (large voxels are required to obtain an adequate signal to noise ratio): the current state of the art achieves a spatial resolution of 6–10 mm in a scan time of about 10–15 min, almost ten times lower than that of CT and MRI and twice than that of PET.

On the other hand, the MR ability to obtain functional and anatomical information at the same examination and without any radiation exposure is an important advantage compared with other imaging techniques.

Biological target characterization by PET

PET imaging permits the assessment of the biomarkers characteristic of a neoplastic cell or related to its activity or its environment. These cellular biomarkers reveal changes in glucose metabolism, amino acid transport and protein synthesis, DNA synthesis, cell proliferation, receptor expression, induction of apoptosis and tumor environment including oxygen status. Thus, PET provides key information that can be exploited to identify different areas of a biologically heterogeneous tumour mass and optimize RTP [27].

The oncological biomarker probe most commonly assessed with PET is the glucose analogue 2-[18F]fluoro-2deoxy-D-glucose ([^{18}F]FDG), which like glucose is transported into cells by glucose transporters (glucs) and then phosphorylated by hexokinase (HK). Tumours generally exhibit increased expression of glucose transporters, especially glut1, and increased activity of HK, especially HK2, thus increasing the rate of uptake and phosphorylation of [^{18}F]FDG. As [^{18}F]FDG phosphate is not a suitable substrate for glucose-6-phosphate isomerase and the level of glucose-6-phosphatase is low in tumours, [^{18}F]FDG phosphate accumulates in tumours allowing their visualization by PET.

PET with [^{18}F]FDG is currently used for tissue characterization and to derive helpful information for patient staging, prognosis, treatment planning and monitoring.

The role of [^{18}F]FDG-PET in oncological patient has been well investigated in non-small cell lung cancers (NSCLC). In a study of Vanuytsel et al. [28], 73 operated patients who had undergone pre-surgery CT and PET/CT scans were examined. CT-based and PET/CT-based mediastinal lymphnode gross tumour volumes (GTVs) were contoured and were compared with surgical pathology data. PET/CT based GTVs showed better concordance with surgical specimen respect to CT (89 vs 75%). In 62% of the patients PET allowed reducing GTV with a potentially diminished toxicity. Comparisons of PET/CT and CT based GTVs without pathologic confirmation has been performed by several investigators. Including PET data has lead to significant changes in mediastinal GTV in percentage of patients varying from 22 to 100% [29–33]. PET caused both an increase and a decrease of the GTV. In some patients, PET allowed discovering previously undetected metastatic disease or nodal spread, thus changing the stage and in some cases also the intent of RT from adjuvant/radical to palliative.

Similar studies were conducted on esophageal cancer. The use of PET/CT resulted in a significant modification of CT-based nodal GTVs in 47–49% [34, 35]; moreover, it allowed detecting unknown metastatic disease.

Also for Hodgkin lymphoma PET-based GTV were different from CT-based ones. In a study by Hutchings [36], PET data led to an increase in CTV in 66% of the patients. Also, in this case, no pathologic data were available.

In a 2004 study [37], Dainse compared CT, MRI, and [^{18}F]FDG-PET GTVs in pharyngo-laryngeal squamous cell carcinoma treatment and validated the results with post-surgical specimen examination. The study concluded that: (1) no modality showed the extent of the primary tumour with complete accuracy; (2) GTVs delineated from [^{18}F]FDG -PET images were the closest to the pathological GTV; (3) the use of CT or MRI led on average to an overestimate of the tumour volume by 40 and 47%, respectively.

Schwartz et al. [38] have reported a pilot study on five patients with different head and neck cancer for whom restricting prophylactic RT to PET positive nodes allowed a better sparing of non-target structures. The potential role of [^{18}F]FDG-PET for rectal cancer RTP [39] or for cervix cancer brachytherapy planning [40] is even more uncertain.

Therefore, [^{18}F]FDG-PET has been shown to influence the selection of target volumes in several diseases. The idea of a biological target volume (BTV) has been proposed but it has not at present been accepted by the ICRU [41].

Moreover, PET can also provide prognostic information. In head and neck patients, a lower [^{18}F]FDG uptake and a decrease in uptake after the first weeks of treatment have both been correlated with a better local control [42]. In rectal cancer, a quantitative assessment of [^{18}F]FDG uptake after chemoradiation has been shown to correlate with long-term survival [43].

IMRT and active scanning hadrontherapy are capable of delivering different doses to different sub-volumes of each single target in a single treatment session. Combining information obtained by one (or more) PET scans with the dose-sculpting ability of modern RT, it would theoretically be possible to selectively deliver a higher dose to those portion of the target that are less likely to be controlled.

Brahme has proposed a very exciting and very complex approach to assess the radiosensitivity of each voxel called BIO-ART (Biologically Optimized 3D in vivo predictive Assay-based Radiation Therapy) [44]. This technique consists in performing a first PET scan before starting RT and a second one after the first week of treatment. A mathematical model have been created to calculate the radioresistance of each voxel and ultimately the dose needed by each voxel to achieve optimal uniform tumor control probability. The model accounts for perfusion, oxygenation, tumour clonogens density, reparable and unreparable damages, cell death and inflammation. This approach has to be considered completely investigational. However, information obtained from PET after an initial course of radiotherapy could provide the basis for continuing with RT treatment vs changing to another (e.g., surgery).

In addition to [^{18}F]FDG, other tracers are and will become available to identify different kinds of tissue processes. A list of tracers employed in RT is given in Table 3 with their most recent published works. The PET tracer (18) F-fluoromisonidazole ([^{18}F]MISO) allows non-invasive assessment of tumour hypoxia, and 3′-deoxy-3′-(18) F-fluorothymidine ([^{18}F]FLT) is developed to investigate tumour cell proliferation. In high-grade gliomas and meningiomas, [^{11}C]methionine PET helps to define the GTV and differentiate tumour from normal tissue. [^{11}C]choline PET signals of the prostate provide adequate spatial information amendable to standardized asymmetrical region growing algorithms for PET-based target volume definition. [^{11}C]acetate PET is another promising tracer in the diagnosis of prostate cancer, but its validity in local tumour demarcation, lymph node diagnosis and detection of recurrence has to be defined in future clinical trials [45].

The development of new PET radiopharmaceuticals may lead in the future to in vivo detection of important tumour biological properties. This would provide further useful information for individualizing cancer treatment.

The main shortcoming of PET imaging is that the exact borders of tumours are not well defined, making visual delineation error-prone. The physician doing the contouring can easily alter the apparent tumour volume on the PET images by simply adjusting the threshold setting. To overcome this problem, dedicated software can automatically create a contour according to a set standardized uptake value (SUV) level [46]. However, there is neither consensus nor a standard procedure for selecting the intensity level to contour a tumour. Open questions include the choice of the threshold in relation to the maximal tumour intensity, as well as the use of a single threshold approach [47]. Jentzen et al. [48] described an interesting iterative thresholding method to estimate PET volumes without anatomic a priori knowledge and its application to clinical images. Another

Table 3 Recent studies addressing the role of PET in high-precision radiotherapy

	PET tracer	Variable	Target	References
Clinical PET studies	[^{18}F]Choline [^{11}C]Choline	Lipid metabolism	Prostate cancer	Ciernik et al. (2007) [104] Yoshida et al. (2005) [105] de Jong et al. (2003) [106]
	[^{11}C]Methionine	Lipid metabolism	Brain tumour	Grosu et al. (2006) [107] Ceyssens et al. (2006) [108] Nariai et al. (2005) [109] Tsuyuguchi et al. (2004) [110] Grosu et al. (2003) [111]
	[^{68}Ga]DOTATOC	Synthesis of proteins	Brain tumour	Milker-Zabel et al. (2006) [112]
	[^{18}F]Fluoromisonidazole ([^{18}F]MISO)	Hypoxia marker	Head-neck cancer; lung-cancer	Thorwarth et al. (2007) [113] Gagel et al. (2006) [114] Thorwarth et al. (2006) [115] Eschmann et al. (2005) [116]
	[^{11}C]Acetate	Cell proliferation marker	Prostate cancer; head and neck	Sun et al. (2007) [117] Oyama et al. (2003) [118] Dehdashti et al. (2003) [119]
	[^{13}N]NH_3	Radiation necrosis	Brain tumour	Xiangsong and Weian (2007) [120]
Pre-clinical PET studies	3′-Deoxy-3′-[^{18}F] Fluorothymidine ([^{18}F]FLT)	Cell proliferation marker	Murine SCCVII tumours	Yang et al. (2006) [121] Sugiyama et al. (2004) [122]
			Model of Esophageal Cancer.	Chao (2007) [123]
	4-borono-2-[^{18}F]-fluoro-1-phenylalanine-fructose ([^{18}F]FBPA-F)	Boron carrier in boron neutron capture therapy (BNCT)	Brain tumour	Chen et al. (2004) [124]

method developed for automatic volume segmentation is based on the relationship between source-to-background ratio and the activity level as described by Daisne et al. [49]. This latter method looks promising in relation to pathologic examination in laryngeal cancer. Because scanning protocols and SUV levels are not yet standardised [50], published data still need to be validated in individual departments before they can be introduced into clinical practice. Furthermore, many other factors affect PET tumour contours: the tumour's metabolic activity, heterogeneity within a tumour and tumour motion [51].

Important technical hurdles of PET employment in RTP are also incapability problems (depending of vendors) in transferring PET images with the picture archiving and communication system (PACS) standard and visualizing real SUV values on the RTP systems (not only tons of colours). The principal obstacles to PACS and PET integration have been listed as [52]: (1) loss of information stored in manufacture's specific private fields; (2) poor support for the PET or nuclear medicine portions of DICOM standard (IODs); (3) the assumption that the PET and nuclear medicine IODs are the same thing; and (4) poor image display design and functionality.

Simultaneous use of multiple imaging modalities and co-registration issues

To be used in RTP, PET and MRI-MRS images must be accurately matched and co-registered with CT images of the treatment simulation. Normally, the CT slices are kept as the standard upon which the other modality images are aligned automatically or interactively.

The motivation for registering studies is to be able to map information from one study to another or to directly combine or fuse the imaging data to create displays that contain relevant features from each modality. For example, a tumour volume may be more clearly visualized using a specific MR image sequence or a coronal image plane rather than axial CT. If the geometric transformation between the MR and the treatment planning CT study is known, the clinician can outline the tumour using images from the MR and then map these outlines onto the CT images. Another approach to combining information from different imaging studies is to directly map the image intensity data from one study onto another so that there are two (or more) intensity values at each voxel instead of one. For example, functional information from a PET scan can be merged or fused with the anatomic information from a CT study and displayed as a colour wash overlay.

Software co-registration methods are now available in most RTP systems. These algorithms could be grouped as feature-based or volume-based methods. Feature-based registration algorithms seek to align corresponding anatomic landmarks, organ surfaces or other features (also with the help of external fiducial markers). A representative example of the feature-based approach is the 'head and hat' method [53]. Volume-based algorithms have been introduced to

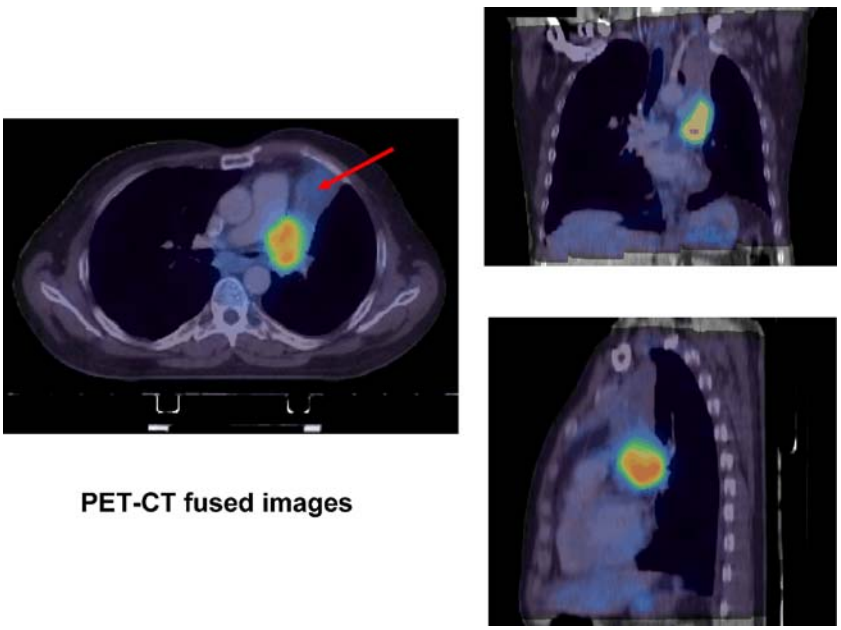

Fig. 2 Co-registration PET and CT data (obtained from separate PET and CT devices) performed on a Hermes workstation, using a normalized mutual information algorithm. The axial, coronal and saggital images belong to a non-small-cell lung cancer patient with atelectasia of the left upper lobe (shown by the *arrow*), which was not part of the target volume. Acquisitions were performed according to the method previously described [103]. Courtesy of Ursula Nestle, Department of Nuclear Medicine, Saarland University Medical Centre, Germany

maximize the similarity (cost function) between images. A representative example of the volume-based approach is the 'mutual information' method [54]. These techniques have been shown to achieve better accuracy than surface-based methods [55] (Fig. 2).

Regarding merging functional with anatomic information, because MRS are acquired using MRI scanners, they are automatically inherently co-registered with the MRI images obtained in the same patient position. MRI and CT co-registered is usually obtained either external fiducial markers that can be seen by both imaging modalities, or using software methods such as the mutual information. Variations to be taken into account are the use of extra coils for MRS examination, such as the endorectal coil used in prostate MRS which adds additional displacement changing to the prostate geometry respect to its treatment position.

For PET, the software co-registration methods can be improved by the use of PET transmission maps or CT images of the integrated PET/CT systems in the cost function because the physiologic variations of the radio-isotope uptake could reduce the accuracy of the co-registration.

Hybrid PET/CT scanners have become widely used in diagnostic oncology applications, but only recently, patients were simulated in radiotherapy position on a dedicated PET/CT simulator with personal immobilisation and patient laser marker system [56]. The alignment accuracy of simulation CT and PET obtained on a hybrid scanner could be higher than that obtained by software co-registration reducing the inconsistency of patient positioning by acquiring functional and anatomical information in the same setting.

Anyway, it should to be taken into account in using PET/CT hybrid scanners that CT data are more rapidly acquired, whereas a PET dataset needs a longer acquisition time, which leads, in turn, to contouring problems. For example, breathing in the thoracic region and bowel and bladder motion in other regions can all produce artefacts. Moreover, for RTP purpose, it could be necessary to acquire CT images in different body configurations for specific purposes (see paragraph below on phase 4), such as in deep inspiration, even when using a hybrid PET/CT system and to co-register the different CT sets with the standard CT images used to attenuation correct the PET emission data.

Recently, Simon Cherry's group has started to develop MR compatible PET detectors at UCLA [57]. The detector principle is based on the use of long optical fibres that guide the light from scintillation crystals positioned within the magnetic field to position sensitive photo-multiplier tubes outside, where the fringe field drops below 10 mT. The light guide is 3–4 m long. Based on this technology, the first simultaneous PET and MR imaging studies of phantoms at 1.5 T were performed with a single-layer lutetium oxyorthosilicate (LSO) ring measuring 54 mm in diameter [58].

The earliest motivation for combined PET/MRI was the fact that strong magnetic fields can reduce the positron range effect. However, significant resolution improvements are realized only at high fields (4.7 T or higher) and only for those positron emitters that emit high-energy positrons. The current motivation appears driven by biomedical applications in certain areas in which MRI is the anatomic imaging modality of choice [59].

In any case, connectivity, compatibility and cooperation between various clinical departments are essential for the successful application of multiple imaging modalities in RTP.

Phase 3: patient set-up verification

In conventional RT, treatment verification was usually done by means of the megavoltage (MV) linear accelerator beam, in high-precision RT more complex approaches are needed.

With high-precision radiotherapy, the treated volume is closely conformed to planning target volume (PTV); outside this volume, the high gradient results in a steep dose decrease. This enhanced conformity reduces the volume of OARs being irradiated; it is therefore more critical to correctly define the range of set-up uncertainties and to give adequate margins from clinical target volume (CTV) to PTV to avert the risk of geometrical misses at some or even all treatment fractions.

A set-up error is the difference between the actual and intended position of the part of the patient that is irradiated. In this section, an overview of imaging devices used to verify and correct set-up errors is given. In conventional approaches, imaging is used to verify set-up errors in the first treatment session after the patient is re-positioned on the accelerator table. In subsequent sessions, the patient is positioned with the aid of lasers and skin marks (tattoos). Depending on the site, imaging can be used for additional verification. In conventional RT, the same MV beam employed for therapy is used to obtain verification images (portal imaging) [60] that are detected through an electronic portal imaging device (EPID). Although faster, EPID is still limited by low subject contrast of bony anatomy at MV energies, large imaging dose, and small radiation fields. With EPID, the accuracy of set-up measurements depends largely on the availability of software for automatic matching of reference images and portal images.

In IGRT, imaging is routinely used for positioning at each treatment session with several technologies. These modalities may be divided into five groups:

1. ultrasonography devices;
2. room-mounted kV X-ray tubes;
3. traditional multi-slice CT scanners integrated 'on rails' with the gantry linear acceleration;

4. kV or MV cone beam CT scanners with flat-panel technology;
5. special promising IGRT techniques combining imaging devices and dose-delivering machines.

Although the technological advances in IGRT can potentially improve clinical outcome, no single technology or strategy exists that is appropriate for all clinical scenarios.

1. Ultrasonography

Ultrasonography (US) is used for daily target localization before treatment, especially for prostate cancer [61], where a significant positional discrepancy of the prostate exists between the static CT image made for planning and dynamic day-to-day condition of the patient [62].

There are at present several dedicated US IGRT systems [63–65]. In these systems, the echo-graphic probe is localized with respect to the treatment isocenter (usually with optoelectronic technologies) so that its 3D position is known; therefore US images obtained with the probe can be precisely referred to 3D planes with a known orientation with respect to room reference coordinates. The system superimposes the critical structures (rectum, bladder and prostate for prostate treatment) outlined in the RTP phase on the US images. Then, a user-friendly interface allows the physician to move these structures on the screen in order to make them fit with their actual position. Dedicated software compares the actual position of the structures outlined with the theoretically expected position obtained from the CT simulation and then calculates and displays the rotational and translational shifts needed to reposition the patient according to the initial set-up (Fig. 3).

US imaging rarely causes the patient any discomfort and has no known long-term side effects. Because the image quality is diminished when there are air gaps or interposed bones, US is not used for lung and brain imaging. The major disadvantage of US in relation to patient set-up evaluation is that since it is impossible to verify the planned field geometry, a second set-up verification technique needs to be used before delivering the dose.

2. Room-mounted kV X-ray tubes

Megavoltage X-rays provide lower quality images (low contrast and spatial resolution) than kV X-rays because of smaller differences in the attenuation coefficient in the human body at MV than at kV energy. This is why kV X-rays are being more and more employed for imaging in the treatment room. In the simplest kV approach, two orthogonal X-rays tubes and corresponding detectors are installed in the treatment room. Once the patient is set-up on the table as planned, two kV X-rays 2D images are acquired. These images are registered and compared with the reference images (DDRs) to determine needed corrections.

Two-dimensional kV imaging performs very well for sites with bony structures, but the necessary imaging contrast for soft tissues is not easy to obtain. One solution is to implant radio-opaque markers into the target prior to treatment [66].

3. CT-on-rails system

An in-room CT (Fig. 4) is a conventional multi-slice kV CT scanner connected via the treatment table with a linear accelerator that can produce 3D images of the patient's anatomy in the exact treatment set-up. The CT scanner is mounted on rails to allow the CT gantry to move over the

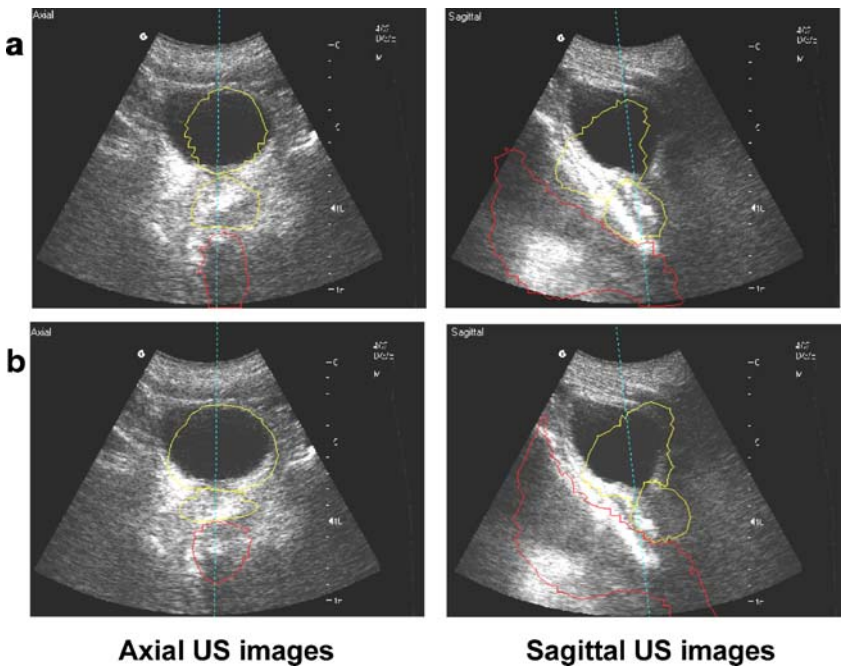

Fig. 3 Axial (*right*) and sagittal (*left*) ultrasound images. The contours in **a** outline the positions of prostate, rectum and bladder as expected from the simulation CT. Contours in **b** have been moved by the operator to fit the actual positions of the organs

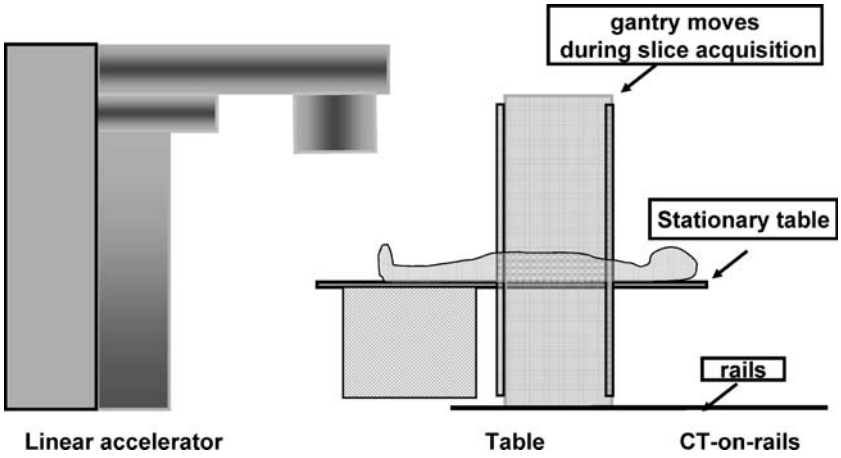

Fig. 4 Illustration of the geometry of an in room CT on-rails integrated with a linear accelerator

patient, instead of having the patient table moving through the gantry, as in typical diagnostic radiology. The CT-on-rails technology was originally developed for intra-operative surgical or interventional guidance to scan without patient motion. After scanning, the treatment couch is rotated to the accelerator side for irradiation. Its accuracy has been demonstrated by Cheng et al. [67].

The CT data set can be also used without any transformation for treatment planning and dose calculation. This makes CT-on-rails well suited for target point verification, correction of setup errors and inter-fraction target deviations due to organ motion, as well as for recalculation of the actually given dose. Systematic changes in the patient's anatomy during therapy (e.g., weight loss, tumour mass reduction) can then be taken into account and the radiation treatment plan re-optimized if necessary [68]. Further investigation needs to be carried out for it to be used in real-time treatment re-optimization because of several remaining issues: integration with routine clinical treatment due to a lack of software tools, frequency of imaging (even in IGRT, a CT scan would not be performed before each treatment fraction), and the cost–efficiency ratio [69].

Clinical experience is still very limited but CT-image-guided radiotherapy appears promising for prostate [70], head and neck cancer [71] and spinal tumours [72].

Because CT scanning is not possible in treatment position and in real time, in principle, this device is not suited for adaptation to intra-fractional variations.

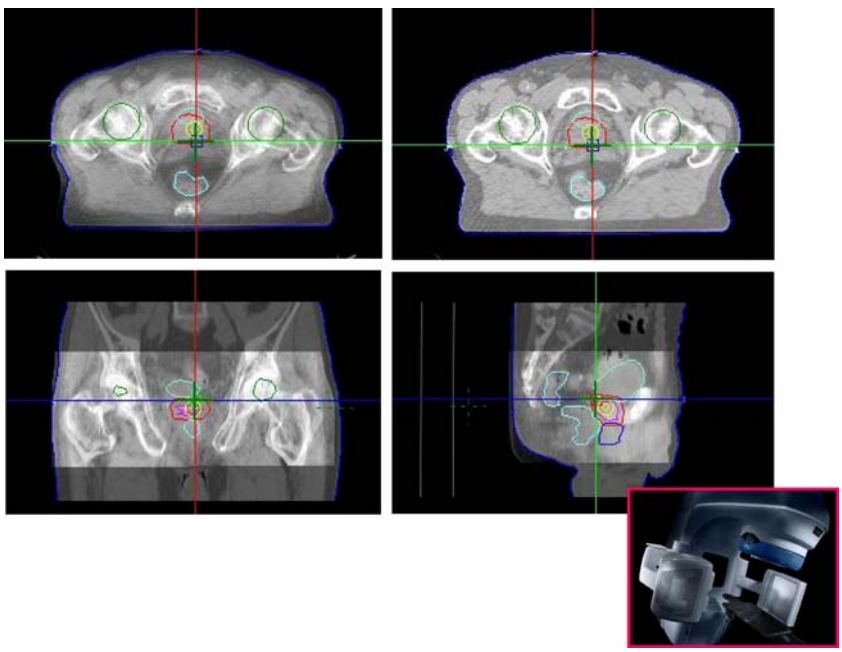

Fig. 5 Representative axial, coronal and sagittal CBCT images (On board imaging, OBI, Varian Medical Systems, Palo Alto, CA, USA) of a patient being treated in the pelvic region using a stereotactic body radiation therapy (SBRT) technique. The images are co-registered with the CT images of the RTP phase

4. KV- or MV-cone beam CT (CBCT)

In the cone beam CT technique, multiple 2D images are obtained by cone shaped X-ray beams from a kV (X-ray tubes) [73] or a MV (linear accelerator beam) source while the gantry rotates around the patient. A 3D image set is then reconstructed using those planar images (Fig. 5) [74].

Owing to the relatively slow gantry rotation (typically about 60 s for a full 360° scan) in acquiring the CBCT projection data, the patient's respiratory motion causes serious problems such as blurring, doubling, streaking and distortion in the reconstructed images, which heavily degrade image quality and target localization [75].

MV-CBCT utilizes the linear acceleration radiation beam and flat panel detector employed for portal imaging to acquire a series of very low-dose 2D projections. These projections are then used to reconstruct the 3D volumetric data set that can be compared with the planning CT [76, 77].

MV-CBCT has displayed superior imaging characteristics in the presence of high Z materials in the imaging field, for example, for head and neck patients with dental work or pelvis patients with a hip prosthesis [89].

5. Special IGRT techniques

All these techniques can be combined with a conventional linear accelerator, but dedicated machines offer tight integration between precise set-up verification and a sophisticated dose delivery system.

The robotic CyberKnife™ from Accuracy (Sunnyvale, CA, USA) represents a special technology that incorporates recent advances in robotics and computerized image recognition [78]. The CyrberKnife mounts a 6-MV lightweight linear accelerator on an industrial robotic arm that accurately (six degrees of freedom) delivers the radiotherapy dose. For real-time digital imaging, two ceiling-mounted diagnostic X-ray cameras with a corresponding orthogonal, floor-mounted amorphous silicon detector are used. These imaging devices can of course be used also with conventional Linacs. The peculiarity of Cyberknife is the close integration between set-up verification and dose delivery. During a single treatment session multiple couples of X-ray images are acquired and are automatically compared with references DRRs. Deviation from the initial set-up position are automatically compensated by the robotic arm.

Helical Tomotherapy (HT) (Fig. 6) is an alternative means of delivering IMRT using a device that combines the features of a linear accelerator with those of a helical CT scanner. The CT images are generated using the same MV radiation beam as the X-ray. The Megavoltage CT thus obtained provide good 3D soft tissues characterization. Because the unit uses the actual treatment beam as the X-ray source for image acquisition, no surrogate telemetry systems are required to register image space to treatment space.

Fig. 6 A commercial HT (Helical Tomotherapy) System. Tomotherapy, Madison, WI, USA. As shown by the figure, this system employs a unique approach to radiation therapy delivery designed as a CT scanner. Before each administration of radiation, a CT scan is performed to precisely target the tumor and avoid nearby critical normal tissues by adjusting the patients' position based on anatomical changes in tumor position, shape or size. Once this adjustment takes place, radiation is administered in a helical fashion

Phase 4: imaging for organ motion and dose delivery monitoring

As discussed above, a major problem in defining target volume and dose delivery is lesion movement resulting from internal organ motion. Temporal anatomic changes can occur for many reasons, but the clinically most relevant is respiration motion during treatment for thoracic and abdominal tumours.

Organ motion

Organ motion is a universal issue in RT but even more relevant in high-precision techniques. IGRT techniques can be used to assess inter-fraction deformation such as those produced by different filling of rectum and bladder, but intra-fraction organ motion demands different more sophisticated approaches.

Cardiac activity and bowel peristalsis can be a source of intra-fraction motion but are minor problems compared to breathing.

In conventional RT, PTV margins are chosen to contain CTV in its excursion during the entire breathing cycle, that is to say that, over the course of treatment, the end expiration and the end inspiration positions of the CTV are always irradiated even though the CTV actually transits in those positions only briefly.

The explicit inclusion of temporal changes in anatomy during the whole RT process (imaging, planning and dose delivery) have led to the development of the four-dimensional (4D) radiotherapy.

In 4D RT, the inclusion of temporal changes in anatomy during radiotherapy, including simulation, planning, as well as dose delivery, reduces PTV margins. To achieve this goal, CTV motion needs to be measured with respect to breathing phases.

Three different approaches are possible:

1. controlled breath hold;
2. respiratory gating;
3. tumour tracking.

1. Controlled breath hold

The patient is instructed to hold his breath during both simulation and treatment delivery. Organ motion is thus abolished during simulation and a static CT image is obtained; to ensure that the procedure is correctly reproduced during treatment delivery, the patient needs to receive feedback (usually a visual signal) that can be either direct measurement of target position by means of fluoroscopy or indirect assessment by measuring other parameters (inhaled volume, optical skin marker position) [79–81].

2. Respiratory gating

In the respiratory gating method, patients breathe freely and treatment is delivered only in a well-defined part of the breathing cycle. To perform gating, a CT acquisition is obtained during free breathing, but each slice is acquired only when the patient is in the correct phase. The signal that triggers CT acquisition is either thoracic wall displacement (measured with optoelectronic technique) or airflow. Dose delivery during treatment is triggered by the same signal that was used for simulation [82–84].

3. Tumour tracking

With this method, patients breathe freely and the delivered field is moved synchronously to follow the CTV in its displacement during the whole breathing cycle [85]. A 4D data set must be acquired during simulation. 4D CT consists of a series of 3D CT image sets acquired at different respiratory phases. Deformable image registration is performed to map each CT image to the corresponding set, considering the peak-inhale respiration phase of each subsequent breath [86].

CT scanning can be adapted to all three approaches, while MRI and PET are usually done only in free breathing. A novel technology has made dynamic MRI of lung motion and lung tumour mobility during continuous respiration feasible with a possible benefit for RT planning [87]. With fast MRI imaging, sample images of the entire lung volume can be obtained fast enough to analyze true motion and deformation during the breathing cycle, whilst the patient breathes freely, as they would during most radiotherapy treatments. Improved MRI technology allows the entire lung to be imaged in a fraction of a second so that organ motion in different breathing cycles can be compared and the variability of the motion assessed in 3D from one cycle to the next. Such studies cannot be carried out using 4D CT, which at present, is formed by acquiring data over many breathing cycles. Spatial correspondence between each of a set of MR image volumes acquired over the breathing cycle is determined using an automatic image registration algorithm.

Standard PET scanning (free breathing) produces an image of the target representing the integral image of the whole volume within which the lesion moves during breathing, with an apparent increase in lesion size and an apparent decrease in activity concentration.

Considerable effort is being focused on the implementation of 4D gated PET/CT acquisition protocols for acquiring PET/CT images synchronized with the patient's breathing curve [88, 89].

Breath holding, gating and tracking techniques have been shown to reduce margins between CTV and PTV and to minimize dose to normal tissue or OAR. During treatment delivery, the target position can be derived by the usual indirect measurement or directly detected with fluoroscopy performed using in-room-mounted kV X-ray [90]. However, fluoroscopic imaging causes a significant amount of extra irradiation of the patient.

New prospects for PET-based dosimetry

Another essential part of high-precision RT is an efficient quality assurance procedure. One exciting area of research in this field is the in vivo verification of the 3D-dose distribution delivered at each treatment session. This can be done with high-energy photons (20 MeV or more) and particles (protons and carbon ions). Such radiations produce β^+-emitting radionuclides by interacting with living matter components during the delivery of RT. This β^+ activity allows PET images to be obtained while the dose is being delivered or immediately after [91]. Although 3D β^+ activity distribution differs from 3D-dose distribution, they are strongly correlated.

In dose distribution evaluation, the use of PET to image β^+ activity distributions induced in the target volume during patient irradiation is currently the most promising technique for in situ, non-invasive dose delivery monitoring. Its use and recent evaluations are discussed below.

A further potential use of PET is to verify the 3D dose distribution delivered during treatment with high-energy photons (20 MeV or more) [92], protons [93] or light ions [94] as they can produce β^+-emitting radionuclides, such as ^{11}C and ^{15}O, by interacting with living matter components.

For almost 30 years, detection of these β^+-emitting radionuclides has stimulated the development of in-beam

PET scanners that can monitor the accuracy of targeting and dose delivery in the treatment room. In-beam PET scanners are systems able to detect photons derived from the β^+ decay of radionuclides formed in the target organs by the incident beams [95]. The use of in-beam PET is preferable to off-beam PET as most of the signal derives from the decay of ^{15}O and ^{11}C, i.e. two rapidly decaying radionuclides ($t_{1/2}$=123 s for ^{15}O and $t_{1/2}$=20.4 min for ^{11}C).

The performance of different types of PET cameras, as well as the results of in-beam PET experiments using beams of β^+ active heavy ions (^{15}O, ^{17}F and ^{19}Ne with energies of 300–500 A MeV), were studied by Pawelke et al. [96]. From the deduced performance, the first dedicated PET scanner for in situ and in vivo treatment plan verification and beam monitoring, as well as dose control during heavy-ion tumour therapy, was constructed at the Gesellschaft für Schwerionenforschung (GSI) in Germany. This scanner is a dual-head positron camera with commercial position sensitive bismuth germanate (BGO) detectors.

The use of a clinically designed scanner has problems related to the low signal to noise ratio from the β^+-emitting radionuclides. Specifically, the limitations are that in-beam PET data are highly corrupted by random coincidences that arise from prompt γ-rays after nuclear reactions of the projectiles with the atomic nuclei of the tissue. They cannot be suppressed with random correction techniques used in conventional PET. Furthermore, the spatial distributions of the delivered dose and of the induced β^+ activity are not congruent. Dedicated procedures have been developed to verify the correct delivery of the treatment plan by means of in-beam PET for monitoring therapy.

Recently, Surti investigated by Monte Carlo simulation the design of a whole-body PET scanner based on new lanthanum bromide ($LaBr_3$) detectors [97]. The results show that there is a gain in signal to noise ratio arising from the reduced scatter and random fractions in a $LaBr_3$ scanner. The reconstructed image resolution is slightly worse than BGO, but at increased count-rates, reduced pulse pileup yields good image resolution, making $LaBr_3$ a promising detector as a basis for in-beam PET scanner.

Ongoing research into the possibility of in vivo dosimetry through portal imaging could be implemented in commercial linear accelerators in the next future [98].

Phase 5: assessment of tumour response

An accepted indicator of successful therapy, included in the Response Evaluation Criteria in Solid Tumours (RECIST), is the decrease in tumour size and lesion enhancement by anatomical imaging (CT or MRI). The size considered is the largest tumour diameter in the axial plane. However, post-treatment morphologic imaging may fail to differentiate between viable tumour and fibrosis, effusion, atelectasis and radiation-induced pneumonitis. Some lesions may persist indefinitely on CT scan, despite the achievement of local control.

Because of the limitations posed by structural imaging modalities on the evaluation of the disease status after RT, the use of functional imaging, most notably [^{18}F]FDG-PET, has been investigated with important outcomes. PET/CT with [^{18}F]FDG has been shown to be highly accurate in determining the viability status of residual post-therapeutic lesions in Hodgkin's diseases and non-Hodgkin's lymphoma, seminoma, head and neck tumours and lung cancer [99].

In addition to [^{18}F]FDG, the use of other radiotracers have been examined for assessing tumour response after radiotherapy, with good results. For example, Molthoff et al. [100] investigated the uptake of [^{18}F]FLT in nude mice bearing xenografts of human head and neck cells, before and during fractionated radiotherapy, to evaluate the potential of [^{18}F]FLT-PET imaging as an indicator of tumour response respect to [^{18}F]FDG.

The use of PET imaging for RT response assessment could be improved not only by the availability of specific radiotracers, but also by the development of dedicated high resolution scanner, such as positron emission mammography (PEM). The PEM combines the quantitative capabilities of PET with millimetre resolution allowing the visualization of the earliest in situ forms of breast cancer as well as putative cancer precursors lesions (e.g., atypical ductal hyperplasia) [101].

However, the optimal timing of post-treatment PET remains undefined. Optimal timing must take into account both the time for resolution of the post-radiotherapy inflammatory response, to minimize false positive results, and the time of residual diseases to reach the thresholds of PET resolution, to minimize false negative studies.

Beside PET imaging, other nuclear medicine techniques have recently been investigated for tumour response assessment after radiotherapy treatment. Ergün et al. [102] studied the role of Tc-99 m (V) dimercaptosuccinic acid (DMSA) scanning in the detection of lung cancer and its metastases, and monitoring the response of tumour lesions to chemo/radiotherapy concluding that single photon emission tomography (SPECT) with DMSA could be applied to all patients for the detection of deeply located lesions.

Today, the role of nuclear medicine techniques in the assessment of tumour response at the end of the RT treatment is established.

Conclusion

Advances in high-precision radiotherapy are closely connected with research into two different areas: volumetric

and temporal multi-modality imaging in treatment planning and assessment response and image-guided radiotherapy before and during dose delivery. These techniques allow organ motion and setup uncertainties to be better measured and controlled during treatment, augmenting accuracy, precision, and overall quality of radiotherapy. This raises the possibility of shortening the duration of RT by reducing the number of treatment sessions (hypo-fractionated radiotherapy). Nonetheless, many issues remain unsolved: optimal organ motion correction during treatment, inter-observer tumour delineation variability, effect of thresholds or other criteria to define tumour margins in PET/CT imaging and optimal timing of post-treatment imaging.

The increasing use of imaging techniques for high-precision RT planning and IGRT and the development of hybrid scanners for target volume definition require through knowledge of all the techniques from imaging specialists working in close connection with radiation therapists, also for optimizing features and dosimetry.

References

1. Fenwick JD, Tome WA, Soisson ET, Mehta MP, Rock Mackie T. Tomotherapy and other innovative IMRT delivery systems. Semin Radiat Oncol 2006;16 4:199–208, Oct.
2. Jereczek-Fossa BA, Krengli M, Orecchia R. Particle beam radiotherapy for head and neck tumors: radiobiological basis and clinical experience. Head Neck 2006;28 8:750–60, Aug.
3. Ling CC, Humm J, Larson S, Amols H, Fuks Z, Leibel S, et al. Towards multidimensional radiotherapy (MD-CRT): biological imaging and biological conformality. Int J Radiat Oncol Biol Phys 2000;47 3:551–60, Jun 1.
4. Dawson LA, Sharpe MB. Image-guided radiotherapy: rationale, benefits, and limitations. Lancet Oncol 2006;7 10:848–58, Oct.
5. Jaffray D, Kupelian P, Djemil T, Macklis RM. Review of image-guided radiation therapy. Expert Rev Anticancer Ther 2007;7 1:89–103, Jan.
6. Sherouse GW, Mosher CE, Novins KL, Rosenmann JG, Chaney EL. Virtual simulation: concept and implementation. In: Bruinvis IAD, van der Giessen PH, van Kleffens HJ, Wittkamper FW, editors. Ninth international conference on the use of computers in radiation therapy. Amsterdam, The Netherlands: North Holland Publishing Co.; 1987, pp. 433–6.
7. Baker GR. Localization: conventional and CT simulation. Br J Radiol 2006;79 Spec No 1:S36–49, Sep.
8. Valentini V, Piermattei A, Morganti AG, Gambacorta MA, Azario L, Macchia G, et al. Virtual simulation: fifteen years later. Rays 2003;28 3:293–8, Jul–Sep.
9. Caldwell CB, Mah K, Ung YC, Danjoux CE, Balogh JM, Ganguli SN, et al. Observer variation in contouring gross tumor volume in patients with poorly defined non-small-cell lung tumors on CT: the impact of 18-FDG-hybrid PET fusion. Int J Radiat Oncol Biol Phys 2001;51:923–31.
10. Cazzaniga LF, Marinoni MA, Bossi A, Bianchi E, Cagna E, Cosentino D, et al. Interphysician variability in defining the planning target volume in the irradiation of prostate and seminal vesicles. Radiother Oncol 1998;47:293–6.
11. Hermans R, Feron M, Bellon E, Dupont P, Van den Bogaert W, Baert AL. Laryngeal tumor volume measurements determined with CT: a study on intra- and interobserver variability. Int J Radiat Oncol Biol Phys 1998;40:553–7.
12. Hurkmans CW, Borger JH, v Giersbergen A, Cho J, Mijnheer BJ. Variability in target volume delineation on CT scans of the breast. Int J Radiat Oncol Biol Phys 2001;50:1366–72.
13. Tai P, Van Dyk J, Yu E, Battista J, Stitt L, Coad T. Variability of target volume delineation in cervical oesophageal cancer. Int J Radiat Oncol Biol Phys 1998;42:277–88.
14. Yamamoto M, Nagata Y, Okajima K, Ishigaki T, Murata R, Mizowaki T, et al. Differences in target outline delineation from CT scans of brain tumours using different methods and different observers. Radiother Oncol 1999;50:151–6.
15. Khoo VS, Joon DL. New developments in MRI for target volume delineation in radiotherapy. Br J Radiol 2006;79 Spec No 1:S2–15, Sep.
16. Lee YK, Bollet M, Charles-Edwards G, Flower MA, Leach MO, McNair H, et al. Radiotherapy treatment planning of prostate cancer using magnetic resonance imaging alone. Radiother Oncol 2003;66 2:203–16, Feb.
17. Thornton AF Jr, Sandler HM, Ten Haken RK, McShan DL, Fraass BA, La Vigne ML, et al. The clinical utility of magnetic resonance imaging in 3-dimensional treatment planning of brain neoplasms. Int J Radiat Oncol Biol Phys 1992;24 4:767–75.
18. Newbold K, Partridge M, Cook G, Sohaib SA, Charles-Edwards E, Rhys-Evans P, et al. Advanced imaging applied to radiotherapy planning in head and neck cancer: a clinical review. Br J Radiol 2006;79 943:554–61, Jul.
19. Manavis J, Sivridis L, Koukourakis MI. Nasopharyngeal carcinoma: the impact of CT-scan and of MRI on staging, radiotherapy treatment planning, and outcome of the disease. Clin Imaging 2005;29 2:128–33, Mar–Apr.
20. Rasch C, Barillot I, Remeijer P, Touw A, van Herk M, Lebesque JV. Definition of the prostate in CT and MRI: a multi-observer study. Int J Radiat Oncol Biol Phys 1999;43 1:57–66, Jan 1.
21. Barillot I, Reynaud-Bougnoux A. The use of MRI in planning radiotherapy for gynaecological tumours. Cancer Imaging 2006;6:100–6, Jun 22.
22. Heenan SD. Magnetic resonance imaging in prostate cancer. Prostate Cancer Prostatic Dis 2004;7 4:282–8.
23. Kauczor HU, Zechmann C, Stieltjes B, Weber MA. Functional magnetic resonance imaging for defining the biological target volume. Cancer Imaging 2006;6:51–5, Jun 1.
24. Zapotoczna A, Sasso G, Simpson J, Roach M. Current role and future perspectives of magnetic resonance spectroscopy in radiation oncology for prostate cancer. Neoplasia 2007;9 6:455–63, Jun.
25. Payne GS, Leach MO. Applications of magnetic resonance spectroscopy in radiotherapy treatment planning. Br J Radiol 2006;79 Spec No 1:S16–26, Sep.
26. Pouliot J, Kim Y, Lessard E, Hsu IC, Vigneron DB, Kurhanewicz J. Inverse planning for HDR prostate brachytherapy used to boost dominant intraprostatic lesions defined by magnetic resonance spectroscopy imaging. Int J Radiat Oncol Biol Phys 2004;59 4:1196–207, Jul 15.
27. Zanzonico P. PET-based biological imaging for radiation therapy treatment planning. Crit Rev Eukaryot Gene Expr 2006;16 1:61–101.
28. Vanuytsel LJ, Vansteenkiste JF, Stroobants SG, De Leyn PR, De Wever W, Verbeken EK, et al. The impact of (18)F-fluoro-2-deoxy-D-glucose positron emission tomography (FDG-PET) lymph node staging on the radiation treatment volumes in patients with non-small cell lung cancer. Radiother Oncol 2000;55 3:317–24, Jun.
29. Erdi YE, Rosenzweig K, Erdi AK, Macapinlac HA, Hu YC, Braban LE, et al. Radiotherapy treatment planning for patients

with non-small cell lung cancer using positron emission tomography (PET). Radiother Oncol 2002;62 1:51–60, Jan.
30. Ashamalla H, Rafla S, Parikh K, Mokhtar B, Goswami G, Kambam S, et al. The contribution of integrated PET/CT to the evolving definition of treatment volumes in radiation treatment planning in lung cancer. Int J Radiat Oncol Biol Phys 2005;63 4:1016–23, Nov 15.
31. Deniaud-Alexandre E, Touboul E, Lerouge D, Grahek D, Foulquier JN, Petegnief Y, et al. Impact of computed tomography and 18F-deoxyglucose coincidence detection emission tomography image fusion for optimization of conformal radiotherapy in non-small-cell lung cancer. Int J Radiat Oncol Biol Phys 2005;63 5:1432–41, Dec 1.
32. Messa C, Ceresoli GL, Rizzo G, Artioli D, Cattaneo M, Castellone P, et al. Feasibility of [18F]FDG-PET and coregistered CT on clinical target volume definition of advanced non-small cell lung cancer. Q J Nucl Med Mol Imaging 2005;49 3:259–66, Sep.
33. Grills IS, Yan D, Black QC, Wong CY, Martinez AA, Kestin LL. Clinical implications of defining the gross tumor volume with combination of CT and 18FDG-positron emission tomography in non-small-cell lung cancer. Int J Radiat Oncol Biol Phys 2007;67 3:709–19, Mar 1.
34. Moureau-Zabotto L, Touboul E, Lerouge D, Deniaud-Alexandre E, Grahek D, Foulquier JN, et al. Impact of CT and 18F-deoxyglucose positron emission tomography image fusion for conformal radiotherapy in esophageal carcinoma. Int J Radiat Oncol Biol Phys 2005;63 2:340–5, Oct 1.
35. Vrieze O, Haustermans K, De Wever W, Lerut T, Van Cutsem E, Ectors N, et al. Is there a role for FGD-PET in radiotherapy planning in esophageal carcinoma? Radiother Oncol 2004;73 3:269–75, Dec.
36. Hutchings M, Loft A, Hansen M, Berthelsen AK, Specht L. Clinical impact of FDG-PET/CT in the planning of radiotherapy for early-stage Hodgkin lymphoma. Eur J Haematol 2007;78 3:206–12, Mar.
37. Daisne JF, Duprez T, Weynand B, Lonneux M, Hamoir M, Reychler H, et al. Tumor volume in pharyngolaryngeal squamous cell carcinoma: comparison at CT, MR imaging, and FDG PET and validation with surgical specimen. Radiology 2004;233 1:93–100, Oct.
38. Schwartz DL, Ford EC, Rajendran J, Yueh B, Coltrera MD, Virgin J, et al. FDG-PET/CT-guided intensity modulated head and neck radiotherapy: a pilot investigation. Head Neck 2005;27 6:478–87, Jun.
39. Gregoire V, Haustermans K, Geets X, Roels S, Lonneux M. PET-based treatment planning in radiotherapy: a new standard? J Nucl Med 2007;48 Suppl 1:68S–77S, Jan.
40. Lin LL, Mutic S, Malyapa RS, Low DA, Miller TR, Vicic M, et al. Sequential FDG-PET brachytherapy treatment planning in carcinoma of the cervix. Int J Radiat Oncol Biol Phys 2005;63 5:1494–501, Dec 1.
41. Schinagl DA, Kaanders JH, Oyen WJ. From anatomical to biological target volumes: the role of PET in radiation treatment planning. Cancer Imaging 2006;6:S107–16, Oct 31.
42. Allal AS, Dulguerov P, Allaoua M, Haenggeli CA, El-Ghazi el A, Lehmann W, et al. Standardized uptake value of 2-[F-18] fluoro-2-deoxy-d-glucose in predicting outcome in head and neck carcinomas treated by radiotherapy with or without chemotherapy. J Clin Oncol 2002;20:1398–404.
43. Kalff V, Duong C, Drummond EG, Matthews JP, Hicks RJ. Findings on 18F-FDG PET scans after neoadjuvant chemoradiation provides prognostic stratification in patients with locally advanced rectal carcinoma subsequently treated by radical surgery. J Nucl Med 2006;47:14–22.
44. Brahme A. Biologically optimized 3-dimensional in vivo predictive assay-based radiation therapy using positron emission tomography-computerized tomography imaging. Acta Oncol 2003;42 2:123–36.
45. Albrecht S, Buchegger F, Soloviev D, Zaidi H, Vees H, Khan HG, et al. (11)C-acetate PET in the early evaluation of prostate cancer recurrence. Eur J Nucl Med Mol Imaging 2007;34 2:185–96, Feb.
46. Erdi YE, Mawlawi O, Larson SM, Imbriaco M, Yeung H, Finn R, et al. Segmentation of lung lesion volume by adaptive positron emission tomography image thresholding. Cancer 1997;80 12 Suppl:2505–9, Dec 15.
47. Biehl KJ, Kong FM, Dehdashti F, Jin JY, Mutic S, El Naqa I, et al. 18F-FDG PET definition of gross tumour volume for radiotherapy of non-small cell lung cancer: is a single standardized uptake value threshold approach appropriate? J Nucl Med 2006;47 11:1808–12.
48. Jentzen W, Freudenberg L, Eising EG, Heinze M, Brandau W, Bockisch A. Segmentation of PET volumes by iterative image thresholding. J Nucl Med 2007;48 1:108–14, Jan.
49. Daisne JF, Sibomana M, Bol A, Doumont T, Lonneux M, Gregoire V. Tri-dimensional automatic segmentation of PET volumes based on measured source-to-background ratios: influence of reconstruction algorithms. Radiother Oncol 2003;69 3:247–50, Dec.
50. Lucignani G, Paganelli G, Bombardieri E. The use of standardized uptake values for assessing FDG uptake with PET in oncology: a clinical perspective. Nucl Med Commun 2004;25 7:651–6, Jul.
51. Erdi YE, Nehmeh SA, Pan T, Pevsner A, Rosenzweig KE, Mageras G, et al. The CT motion quantitation of lung lesions and its impact on PET-measured SUVs. J Nucl Med 2004;45 8:1287–92, Aug.
52. Somer EJ. PACS man: questioning nuclear medicine and PET integration. Nucl Med Commun 2006;27 8:601–2, Aug.
53. Polizzari CA, Chen GT, Spelbring DR, Weichselbaum RR, Chen CT. Accurate three-dimensional registration of CT, PET, and/or MR images of the brain. J Comput Assist Tomogr 1989;13:20–26, Aug.
54. Wells WM, Viola P, Atsumi H, Nakajima S, Kikinis R. Multimodal volume registration by maximization of mutual information. Med Image Anal 1996;1 1:35–51, Mar.
55. Slomka PJ. Software approach to merging molecular with anatomic information. J Nucl Med 2004;45 Suppl 1:36S–45S, Jan.
56. De Ruysscher D, Wanders S, Minken A, Lumens A, Schiffelers J, Stultiens C, et al. Effects of radiotherapy planning with a dedicated combined PET-CT-simulator of patients with non-small cell lung cancer on dose limiting normal tissues and radiation dose-escalation: a planning study. Radiother Oncol 2005;77 1:5–10, Oct.
57. Shao Y, Cherry SR, Farahani K, Slates R, Silverman RW, Meadors K, et al. Development of a PET detector system compatible with MRI/NMR systems. IEEE Trans Nucl Sci 1997;44:1167–71.
58. Farahani K, Slates R, Shao Y, Silverman R, Cherry S. Contemporaneous positron emission tomography and MR imaging at 1.5 T. J Magn Reson Imaging 1999;9 3:497–500, Mar.
59. Catana C, Wu Y, Judenhofer MS, Qi J, Pichler BJ, Cherry SR. Simultaneous acquisition of multislice PET and MR images: initial results with a MR-compatible PET scanner. J Nucl Med 2006;47 12:1968–76, Dec.
60. Hurkmans CW, Remeijer P, Lebesque JV, Mijnheer BJ. Set-up verification using portal imaging; review of current clinical practice. Radiother Oncol 2001;58 2:105–20, Feb.

61. Peignaux K, Crehange G, Truc G, Barillot I, Naudy S, Maingon P. High precision radiotherapy with ultrasonic imaging guidance. Cancer Radiother 2006;10 5:231–4, Sep.
62. Kupelian PA, Langen KM, Willoughby TR, Wagner TH, Zeidan OA, Meeks SL. Daily variations in the position of the prostate bed in patients with prostate cancer receiving postoperative external beam radiation therapy. Int J Radiat Oncol Biol Phys 2006;66 2:593–6, Oct 1.
63. Meeks SL, Buatti JM, Bouchet LG, Bova FJ, Ryken TC, Pennington EC, et al. Ultrasound-guided extracranial radiosurgery: technique and application. Int J Radiat Oncol Biol Phys 2003;55 4:1092–101, Mar 15.
64. Morr J, DiPetrillo T, Tsai JS, Engler M, Wazer DE. Implementation and utility of a daily ultrasound-based localization system with intensity-modulated radiotherapy for prostate cancer. Int J Radiat Oncol Biol Phys 2002;53 5:1124–9, Aug 1.
65. Peignaux K, Truc G, Barillot I, Ammor A, Naudy S, Crehange G, et al. Clinical assessment of the use of the Sonarray system for daily prostate localization. Radiother Oncol 2006;81 2:176–8, Nov.
66. Soete G, De Cock M, Verellen D, Michielsen D, Keuppens F, Storme G. X-ray-assisted positioning of patients treated by conformal arc radiotherapy for prostate cancer: comparison of setup accuracy using implanted markers versus bony structures. Int J Radiat Oncol Biol Phys 2007;67 3:823–7, Mar 1.
67. Cheng CW, Wong J, Grimm L, Chow M, Uematsu M, Fung A. Commissioning and clinical implementation of a sliding gantry CT scanner installed in an existing treatment room and early clinical experience for precise tumor localization. Am J Clin Oncol 2003;26 3:e28–36, Jun.
68. Thieke C, Malsch U, Schlegel W, Debus J, Huber P, Bendl R, et al. Kilovoltage CT using a linac-CT scanner combination. Br J Radiol 2006;79 Spec No 1:S79–86, Sep.
69. de Crevoisier R, Kuban D, Lefkopoulos D. Image-guided radiotherapy by in-room CT-linear accelerator combination. Cancer Radiother 2006;10 5:245–51, Sep.
70. Wong JR, Grimm L, Uematsu M, Oren R, Cheng CW, Merrick S, et al. Image-guided radiotherapy for prostate cancer by CT-linear accelerator combination: prostate movements and dosimetric considerations. Int J Radiat Oncol Biol Phys 2005;61 2:561–9, Feb 1.
71. Barker JL Jr, Garden AS, Ang KK, O'Daniel JC, Wang H, Court LE, et al. Quantification of volumetric and geometric changes occurring during fractionated radiotherapy for head-and-neck cancer using an integrated CT/linear accelerator system. Int J Radiat Oncol Biol Phys 2004;59 4:960–70, Jul 15.
72. Chang EL, Shiu AS, Lii MF, Rhines LD, Mendel E, Mahajan A, et al. Phase I clinical evaluation of near-simultaneous computed tomographic image-guided stereotactic body radiotherapy for spinal metastases. Int J Radiat Oncol Biol Phys 2004;59 5:1288–94, Aug 1.
73. Oelfke U, Tucking T, Nill S, Seeber A, Hesse B, Huber P, et al. Linac-integrated kV-cone beam CT: technical features and first applications. Med Dosim 2006;31 1:62–70, Spring.
74. Sorcini B, Tilikidis A. Clinical application of image-guided radiotherapy, IGRT (on the Varian OBI platform). Cancer Radiother 2006;10 5:252–7, Sep.
75. Li T, Schreibmann E, Yang Y, Xing L. Motion correction for improved target localization with on-board cone-beam computed tomography. Phys Med Biol 2006;51 2:253–67, Jan 21.
76. Mosleh-Shirazi MA, Evans PM, Swindell W, Webb S, Partridge M. A cone-beam megavoltage CT scanner for treatment verification in conformal radiotherapy. Radiother Oncol 1998;48 3:319–28, Sep.
77. Pouliot J, Bani-Hashemi A, Chen J, Svatos M, Ghelmansarai F, Mitschke M, et al. Low-dose megavoltage cone-beam CT for radiation therapy. Int J Radiat Oncol Biol Phys 2005;61 2:552–60, Feb 1.
78. Kuo JS, Yu C, Petrovich Z, Apuzzo ML. The CyberKnife stereotactic radiosurgery system: description, installation, and an initial evaluation of use and functionality. Neurosurgery 2003;53 5:1235–9, Nov.
79. Wong JW, Sharpe MB, Jaffray DA, Kini VR, Robertson JM, Stromberg JS, et al. The use of active breathing control (ABC) to reduce margin for breathing motion. Int J Radiat Oncol Biol Phys 1999;44 4:911–9, Jul 1.
80. Mah D, Hanley J, Rosenzweig KE, Yorke E, Braban L, Ling CC, et al. Technical aspects of the deep inspiration breath-hold technique in the treatment of thoracic cancer. Int J Radiat Oncol Biol Phys 2000;48 4:1175–85, Nov 1.
81. Mageras GS, Yorke E. Deep inspiration breath hold and respiratory gating strategies for reducing organ motion in radiation treatment. Semin Radiat Oncol 2004;14 1:65–75, Jan.
82. Minohara S, Kanai T, Endo M, Noda K, Kanazawa M. Respiratory gated irradiation system for heavy-ion radiotherapy. Int J Radiat Oncol Biol Phys 2000;47 4:1097–103, Jul 1.
83. Kubo D, Hill BC. Respiration gated radiotherapy treatment: a technical study. Physics 1996;41 1:83–91, Jan.
84. Kubo D, Len PM, Minohara S, Mostafavi H. Breathing synchronized radiotherapy program at the University of California Davis Cancer Center. Med Phys 2000;27 2:346–53, Feb.
85. Onimaru R, Shirato H, Fujino M, Suzuki K, Yamazaki K, Nishimura M, et al. The effect of tumor location and respiratory function on tumor movement estimated by real-time tracking radiotherapy (RTRT) system. Int J Radiat Oncol Biol Phys 2005;63 1:164–9, Sep 1.
86. Keall PJ, Joshi S, Vedam SS, Siebers JV, Kini VR, Mohan R. Four-dimensional radiotherapy planning for DMLC-based respiratory motion tracking. Med Phys 2005;32 4:942–51, Apr.
87. Kauczor HU, Plathow C. Imaging tumour motion for radiotherapy planning using MRI. Cancer Imaging 2006;6:S140–4, Oct 31.
88. Nehmeh SA, Erdi YE, Pan T, Pevsner A, Rosenzweig KE, Yorke E, et al. Four-dimensional (4D) PET/CT imaging of the thorax. Med Phys 2004;31 12:3179–86, Dec.
89. Wolthaus JW, van Herk M, Muller SH, Belderbos JS, Lebesque JV, de Bois JA, et al. Fusion of respiration-correlated PET and CT scans: correlated lung tumour motion in anatomical and functional scans. Phys Med Biol 2005;50 7:1569–83, Apr 7.
90. Willoughby TR, Forbes AR, Buchholz D, Langen KM, Wagner TH, Zeidan OA. Evaluation of an infrared camera and X-ray system using implanted fiducials in patients with lung tumors for gated radiation therapy. Int J Radiat Oncol Biol Phys 2006;66 2:568–75, Oct 1.
91. Parodi K, Paganetti H, Cascio E, Flanz JB, Bonab AA, Alpert NM, et al. PET/CT imaging for treatment verification after proton therapy: a study with plastic phantoms and metallic implants. Med Phys 2007;34 2:419–35, Feb.
92. Mockel D, Muller H, Pawelke J, Sommer M, Will E, Enghardt W. Quantification of beta(+) activity generated by hard photons by means of PET. Phys Med Biol 2007;52 9:2515–30, May 7.
93. Parodi K, Enghardt W, Haberer T. In-beam PET measurements of β^+ radioactivity induced by proton beams. Phys 2002;47 1:21–36, Jan 7.
94. Ponisch F, Parodi K, Hasch BG, Enghardt W. The modelling of positron emitter production and PET imaging during carbon ion therapy. Phys Med Biol 2004;49 23:5217–32, Dec 7.
95. Enghardt W, Fromm WD, Geissel H, Heller H, Kraft G, Magel A, et al. The spatial distribution of positron-emitting nuclei generated by relativistic light ion beams in organic matter. Phys Med Biol 1992;37:2127.

96. Pawelke J, Byars L, Enghardt W, Fromm WD, Geissel H, Hasch BG, et al. The investigation of different cameras for in-beam PET imaging. Phys Med Biol 1996;41:279–96.
97. Surti S, Karp JS, Muehllehner G. Image quality assessment of LaBr3-based whole-body 3D PET scanners: a Monte Carlo evaluation. Phys Med Biol 2004;49 19:4593–610, Oct 7.
98. Piermattei A, Fidanzio A, Stimato G, Azario L, Grimaldi L, D'Onofrio G, et al. In vivo dosimetry by an aSi-based EPID. Med Phys 2006;33 11:4414–22, Nov.
99. Messa C, Di Muzio N, Picchio M, Gilardi MC, Bettinardi V, Fazio F. PET/CT and radiotherapy. Q J Nucl Med Mol Imaging 2006;50 1:4–14, Mar.
100. Molthoff CF, Klabbers BM, Berkhof J, Felten JT, van Gelder M, Windhorst AD, et al. Monitoring Response to Radiotherapy in Human Squamous Cell Cancer Bearing Nude Mice: Comparison of 2′-deoxy-2′-[(18)F]fluoro-D-glucose (FDG) and 3′-[(18)F] fluoro-3′-deoxythymidine (FLT). Mol Imaging Biol 2007, Jul 21, in press.
101. Weinberg IN. Applications for positron emission mammography. Phys Med 2006;21 Suppl 1:132–7.
102. Ergün EL, Kara PO, Gedik GK, Kars A, Turker A, Caner B. The role of Tc-99m (V) DMSA scintigraphy in the diagnosis and follow-up of lung cancer lesions. Ann Nucl Med 2007;21 5:275–83, Jul.
103. Nestle U, Schaefer-Schuler A, Kremp S, Groeschel A, Hellwig D, Rube C, et al. Target volume definition for 18F-FDG PET-positive lymph nodes in radiotherapy of patients with non-small cell lung cancer. Eur J Nucl Med Mol Imaging 2007;34 4:453–62, Apr.
104. Ciernik IF, Brown DW, Schmid D, Hany T, Egli P, Davis JB. 3D-segmentation of the (18)F-choline PET signal for target volume definition in radiation therapy of the prostate. Technol Cancer Res Treat 2007;6 1:23–30, Feb.
105. Yoshida S, Nakagomi K, Goto S, Futatsubashi M, Torizuka T. 11C-Choline positron emission tomography in prostate cancer: primary staging and recurrent site staging. Urol Int 2005;74:214–20.
106. de Jong IJ, Pruim J, Elsinga PH, Vaalburg W, Mensink HJ. 11C-choline positron emission tomography for the evaluation after treatment of localized prostate cancer. Eur Urol 2003;44 1:32–8, Jul.
107. Grosu AL, Weber WA, Astner ST, Adam M, Krause BJ, Schwaiger M, et al. 11C-methionine PET improves the target volume delineation of meningiomastreated with stereotactic fractionated radiotherapy. Int J Radiat Oncol Biol Phys 2006;66 2:339–44, Oct 1.
108. Ceyssens S, Van Laere K, de Groot T, Goffin J, Bormans G, Mortelmans L. [11C]methionine PET, histopathology, and survival in primary brain tumors and recurrence. AJNR Am J Neuroradiol 2006;27 7:1432–7, Aug.
109. Nariai T, Tanaka Y, Wakimoto H, Aoyagi M, Tamaki M, Ishiwata K, et al. Usefulness of L-[methyl-11C] methionine-positron emission tomography as a biological monitoring tool in the treatment of glioma. Neurosurgery 2005;103 3:498–507, Sep.
110. Tsuyuguchi N, Takami T, Sunada I, Iwai Y, Yamanaka K, Tanaka K, et al. Ann methionine positron emission tomography for differentiation of recurrent brain tumor and radiation necrosis after stereotactic radiosurgery-in malignant glioma. Nucl Med 2004;18 4:291–6, Jun.
111. Grosu AL, Lachner R, Wiedenmann N, Stark S, Thamm R, Kneschaurek P, et al. Validation of a method for automatic image fusion (BrainLAB System) of CT data and 11Cmethionine-PET data for stereotactic radiotherapy using a LINAC: first clinical experience. Int J Radiat Oncol Biol Phys 2003;56 5:1450–63, Aug 1.
112. Milker-Zabel S, Zabel-du Bois A, Henze M, Huber P, Schulz-Ertner D, Hoess A, et al. Improved target volume definition for fractionated stereotactic radiotherapy in patients with intracranial meningiomas by correlation of CT, MRI, and [68Ga]-DOTA-TOC-PET. Int J Radiat Oncol Biol Phys 2006;65 1:222–7, May 1.
113. Thorwarth D, Eschmann S, Paulsen F, Alber M. A model of reoxygenation dynamics of head-and-neck tumors based on serial 18F-fluoromisonidazole positron emission tomography investigations. Int J Radiat Oncol Biol Phys 2007;68 2:515–21, Jun 1.
114. Gagel B, Reinartz P, Demirel C, Kaiser HJ, Zimny M, Piroth M, et al. BMC [18F] fluoromisonidazole and [18F] fluorodeoxyglucose positron emission tomography in response evaluation after chemo-/radiotherapy of non-small-cell lung cancer: a feasibility study. Cancer 2006;6:51, Mar 4.
115. Thorwarth D, Eschmann SM, Holzner F, Paulsen F, Alber M. Combined uptake of [18F]FDG and [18F]FMISO correlates with radiation therapy outcome in head-and-neck cancer patients. Radiother Oncol 2006;80 2:151–6, Aug.
116. Eschmann SM, Paulsen F, Reimold M, Dittmann H, Welz S, Reischl G, et al. Prognostic impact of hypoxia imaging with 18F-misonidazole PET in non-small cell lung cancer and head and neck cancer before radiotherapy. J Nucl Med 2005;46 2:253–60, Feb.
117. Sun A, Sorensen J, Karlsson M, Turesson I, Langstrom B, Nilsson P, et al. 1-[11C]-acetate PET imaging in head and neck cancer-a comparison with 18F-FDG-PET: implications for staging and radiotherapy planning. Eur J Nucl Med Mol Imaging 2007;34 5:651–7, May.
118. Oyama N, Miller TR, Dehdashti F, Siegel BA, Fischer KC, Michalski JM, et al. 11Cacetate PET imaging of prostate cancer: detection of recurrent disease at PSA relapse. J Nucl Med 2003;44 4:549–55, Apr.
119. Dehdashti F, Siegel BA, Fischer KC, Michalski JM, Kibel AS, Andriole GL, et al. 11Cacetate PET imaging of prostate cancer: detection of recurrent disease at PSA relapse Oyama N. Miller J Nucl Med 2003;44 4:549–55, Apr.
120. Xiangsong Z, Weian C. Differentiation of recurrent astrocytoma from radiation necrosis: a pilot study with (13)N-NH (3) PET. J Neurooncol 2007;82 3:305–11, May.
121. Yang YJ, Ryu JS, Kim SY, Oh SJ, Im KC, Lee H, et al. Use of 3′-deoxy-3′-[18F]fluorothymidine PET to monitor early responses to radiation therapy in murine SCCVII tumors. Eur J Nucl Med Mol Imaging 2006;33 4:412–9, Apr.
122. Sugiyama M, Sakahara H, Sato K, Harada N, Fukumoto D, Kakiuchi, et al. Evaluation of 3′-Deoxy-3′-18F-fluorothymidine for monitoring tumor response to radiotherapy and photodynamic therapy in mice. J Nucl Med 2004;45 10:1754–8, Oct.
123. Chao KS. 3′-deoxy-3′-(18)F-fluorothymidine (FLT) Positron emission tomography for early prediction of response to chemo-radiotherapy—a clinical application model of esophageal cancer. Semin Oncol 2007;34 2 Suppl 1:S31–6, Apr.
124. Chen JC, Chang SM, Hsu FY, Wang HE, Liu RS. MicroPET-based pharmacokinetic analysis of the radiolabeled boron compound [18F]FBPA-F in rats with F98 glioma. Appl Radiat Isot 2004;61 5:887–91, Nov.